Engineering Structures 260 (2022) 114202

Contents lists available at ScienceDirect

Engineering Structures

journal homepage: www.elsevier.com/locate/engstruct

Experimental and numerical investigation of lightweight foamed reinforced concrete deep beams with steel fibers☆

Mohamed S. Manharawy [a], Ahmed A. Mahmoud [b,*], Osama O. El-Mahdy [b], Mosaad H. El-Diasity [b]

[a] Higher Institute of Enginee ing, 15th of May City, Egypt
[b] Faculty of Engineering at Shoubra, Benha University, Egypt

ARTICLE INFO

Keywords:
Lightweight foamed reinforced concrete
Deep beams
Steel fibers
Shear capacity
Experimental
Numerical, strut-and tie model

ABSTRACT

This paper aims to experimentally and numerically study the effect of steel fiber on the behavior of Lightweight Foamed Reinforced Concrete (LWFRC) deep beams and its mechanism to improve the mechanical properties and crack control of concrete. In addition to this, steel fibers compensate for the lack of resistance due to the use of lightweight foamed concrete (LWFC). This paper will also address the effect of some variable parameters on the structural behavior such as: (1) volume of fiber; (2) fiber aspect ratio; (3) longitudinal reinforcement ratio.

The experimental program consists of four groups; each group comprises two beams compared to the control specimen. All beams have an overall depth of 800 mm, width of 150 mm, and total length of 2200 mm with span of 2000 mm. Tests were performed under two points load with constant shear-span to depth ratio equal to one. The used LWFC has an average cubic, cylindrical compressive strength and splitting tensile strength of 33, 28 and 3.10 MPa, respectively. Hooked end steel fibers with length 40, 50, and 60 mm and 0.8 mm diameter were used with 0%, 0.5%, 0.75% and 1.0% volumetric ratio.

The obtained results indicated that the cracking and the ultimate load has increased by 18.5% and 25.5%, respectively due to use steel fibers. Furthermore, the displacement ductility and toughness has increased by 38% and 56%, respectively. The failure mode of LWFRC deep beams is shear brittle failure.

Shear capacity of all deep beams based on ECP 203–2017 (ECP-203, 2017) is calculated and compared with that from ACI 318–19 (ACI 318-19, 2018) which is based on strut and tie model (STM). Comparing the experimental results with STM results showed that ECP 203–2017 (ECP-203, 201) is slightly conservative in calculating the ultimate capacity than ACI 318–19 (ACI 318-19, 2018) for the range of the studied variables in this research and not in general. Finally, as the STMs are debatable, ANSYS 15 software was used to numerically study the behavior of LWFRC deep beams. Verification of numerical models has been done by comparing the results of the load deflection curves, cracks and ultimate loads with the experimental ones.

1. Introduction

There are many shapes and types of lightweight concrete (LWC), one of them is the foamed concrete which is being widely used in construction [3,4]. LWFC can be used for structural purposes after enhancing its performance. LWFC has the following properties: (1) high thermal insulation properties; (2) flowability; (3) self-compacting; and (4) speed of construction [5,6]. Moreover, foamed concrete has low densities, ranging from 400 to 1850 kg/m^3 [7,8]. Scholar [9] used foamed concrete and carried out many trials for two suggested mixtures with and without sand, where the compressive strength after 28-days was 17.0 MPa. Hilal et al. [10] performed an experimental study on enhanced foamed concrete with densities from 1300 to 1900 kg/m^3 using silica fume and fly ash. Sika air product from Sika company with foam creates air bubbles and porous microstructure by entrapment of air bubbles in the concrete mix. The air bubbles diameter ranges from 0.1 and 1.0 mm. The air bubbles size and shape remain stable for the period

☆ This research did not receive any specific grant from funding agencies in the public, commercial, or not-for-profit sectors.
* Corresponding author at: Department of Civil Engineering, Faculty of Engineering at Shoubra, Benha University, 108 Shoubra Street, Shoubra 11691, Cairo, Egypt.
E-mail addresses: ahmed.ahmed@feng.bu.edu.eg (A.A. Mahmoud), osama.alhenawy@feng.bu.edu.eg (O.O. El-Mahdy), mosaad.ali@feng.bu.edu.eg (M.H. El-Diasity).

https://doi.org/10.1016/j.engstruct.2022.114202
Received 7 June 2021; Received in revised form 18 March 2022; Accepted 26 March 2022

Nomenclature

a	is the shear span (the distance from the load to the support constant at 800 mm);
A_s‘	is the compression steel reinforcement (constant at 2 Φ 10);
b	is the beam width (constant at 150 mm);
f_{cu}	is the cubic concrete compressive strength (average value 33 MPa);
f'_c	is the cylindrical concrete compressive strength (average value 28 MPa);
f_t	is the experimental concrete tensile strength (average value 3.10 MPa);
L_o	is the beam clear span (constant at 2000 mm);
L_0/t	is the beam clear span to total depth ratio (constant at 2.5);
L_f/ Φ_f	is the steel fibers aspect ratio (length of fiber/diameter of fiber 50, 62.5 and 75);
$P_{crf\ exp.}$	is the experimental load at first flexural crack;
$P_{crf\ FE}$	is the predicted load at first flexural crack from finite element analysis;
$P_{crs\ exp.}$	is the experimental load at first diagonal shear crack;
$P_{crs\ FE}$	is the predicted load at first diagonal shear crack from finite element analysis;
$P_{u\ exp.}$	is the experimental ultimate load;
$P_{u\ FE}$	is the predicted ultimate load from finite element analysis;
$P_{u\ STM}$	is the predicted ultimate load from strut and tie model (STM);
S_v	is the spacing between the vertical stirrups (constant at 75 mm);
S_h	is the spacing between the horizontal web reinforcement (constant at 75 mm);
t	is the total depth of the beam (constant at 800 mm);
a/t	is the share- span to total depth ratio (constant at 1.0);
V_f %	is the steel fibers volumetric percent relative to concrete volume (0.0,0.5 %,0.75 % and 1.0 %);
$\Delta_{u\ exp.}$	is the measured ultimate deflection;
$\Delta_{u\ FE.}$	is the predicted ultimate deflection from finite element analysis;
μ	is the ratio of the main reinforcement steel (area of main reinforcement steel/area of concrete);
μ_{max}	is the maximum reinforcement steel ratio according to ECP 203–2017 [1];
μ_v%	is the percentage of the vertical web reinforcement (constant at 1.12%);
μ_h%	and is the percentage of the horizontal web reinforcement (constant at 1.12%).

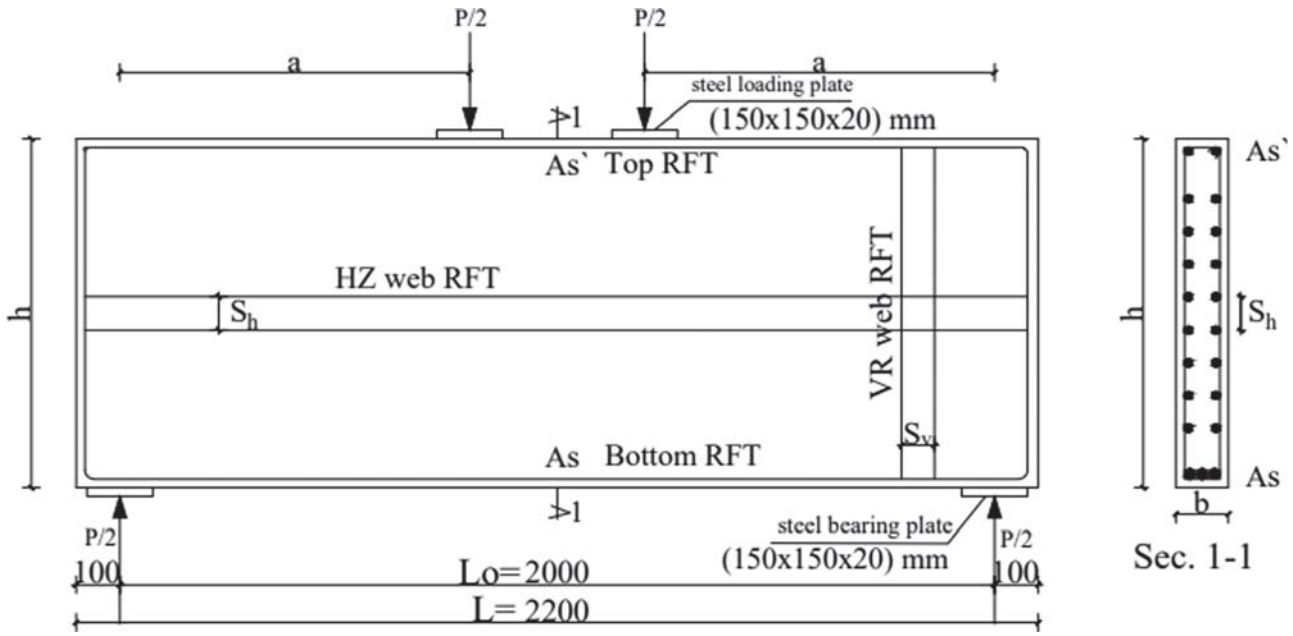

Fig. 1. Symbols and notations.

of the setting process [11-19].

With the inclusion of steel fibers in LWFC, it increases the flexural, tensile strength, the resistance to dynamic and sudden loading and the strength against explosive effects. Incorporation of steel fibers in LWFC increases its load carrying capacity to be closer to the strength of normal weight concrete. This also controls the propagation of cracks and decreases the crack width. Moreover, the ability of deformation is decreased achieving economical solutions through reducing the weight of the concrete [20-23].

Pujadas et al. [24] used steel fibers in concrete mixture due to creep behavior; where it has time-dependent strain that develops in concrete due to sustained stress.

Song and Hwang [25] investigated the mechanical properties of high-strength steel fibers-reinforced concrete. The properties included compressive and splitting tensile strengths, modulus of rupture, and toughness index. Yazici et al. [26] experimentally studied the effects of aspect ratio (L_f/ Φ_f) and volume fraction (V_f) of steel fibers on the compressive strength, split tensile strength, flexural strength and ultrasonic pulse velocity of steel fibers reinforced concrete (SFRC). It was concluded that the inclusion of steel fibers significantly affects the split tensile and flexural strength of concrete in accordance with (L_f/ Φ_f) ratio and (V_f).

Hao and Hong [27] studied pull-out behavior of spiral steel fibers from normal-strength concrete and significant improvement by the

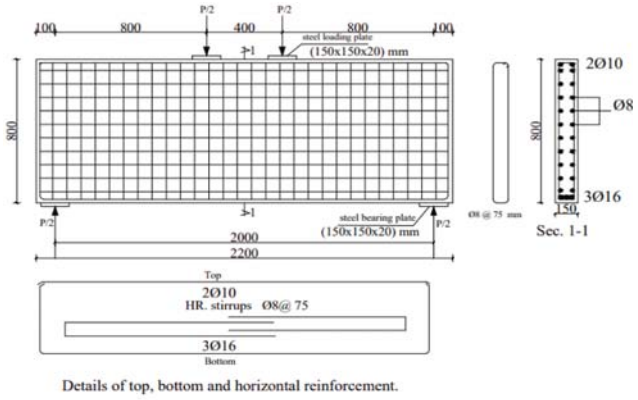

Details of top, bottom and horizontal reinforcement.

(a) Beams B1, B2, B5, B6, B7 and B8.

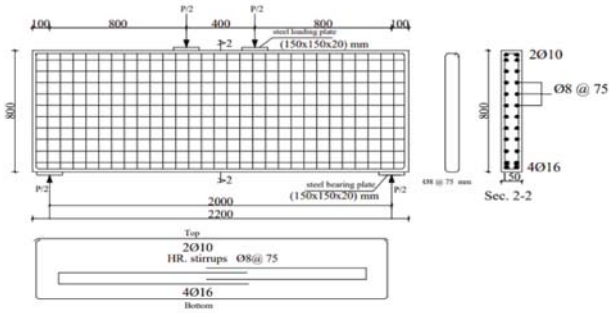

Details of top, bottom and horizontal reinforcement.

(b) Beam B3.

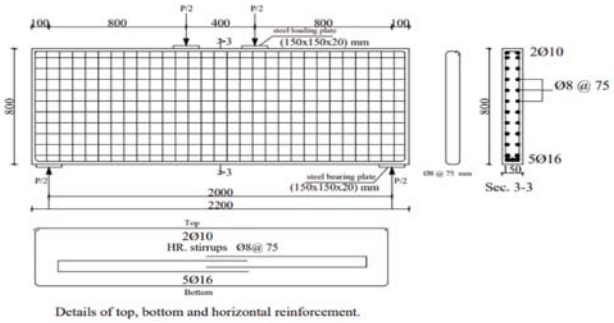

Details of top, bottom and horizontal reinforcement.

(c) Beam B4.

Fig. 2. Details and dimensions of tested beams. (All dimensions are in mm).

Table 1
Data of the tested beams.

Group No.	Beam No.	V_f%	l_f/ϕ_f	Main reinforcement	μ / μ max
1	B1	0.00	0	3 Φ 16	0.30
	B2	0.50	62.5	3 Φ 16	0.30
2	B3	0.50	62.5	4 Φ 16	0.40
	B4	0.50	62.5	5 Φ 16	0.50
3	B5	0.75	62.5	3 Φ 16	0.30
	B6	1.00	62.5	3 Φ 16	0.30
4	B7	0.50	75	3 Φ 16	0.30
	B8	0.50	50	3 Φ 16	0.30

synergistic effect of hybrid fibers was demonstrated. Shengli et al. [28] studied the effect of fiber orientation and content on tensile strength of SFRC. Raju et al. [29] experimentally investigated the effects of concrete type, fiber content, and specimen depth on the fiber distribution, orientation and the structural performance of SCFRC and SFRC beams considering their fiber distribution and orientation. Gou et al. [30] designed a novel device and method to orientally distribute thin and short steel fibers in ultra-high-performance concrete (UHPC) and the results demonstrated that the mechanical properties such as flexural strength, flexural-tensile strength, flexural toughness, and interfacial bonding strength of UHPC were improved.

The behavior of deep beams is different from that of conventional beams; where it requires special consideration in analysis and design, in addition to detailing of reinforcement [31-34].

Conventional shear reinforcement (vertical and horizontal shear reinforcement (stirrups)) is unable to provide efficient resistance to cracks formation and propagation under the effect of external loading [35]. Magdalene, P.S. and Kanmani, V., [36], verified the experimental study of reinforced concrete deep beams with compressive strength of 20 MPa (M20 grade) and different length to depth ratios (1.5, 2.0 and 2.5), and ANSYS 9.0 was used to analyze the results. Many researchers have studied deep beams and concluded their design method, using strut and tie method [37-43].

Hassani et al. [44] compared the cracking moment and modulus of rupture in deep and normal beams. The results showed that in deep beams, the corresponding load to the occurrence of the first crack is around two times more than in normal beams. Jang et al. [45] investigated the effects of using steel fibers as transverse reinforcement on the seismic performance of diagonally reinforced coupling beams that are composed of normal- and high-strength concrete. The results showed that the inclusion of steel fibers has improved flexural behavior and toughness of concrete.

Albidah et al. [46] experimentally and analytically investigated the effectiveness of the adopted schemes for strengthening of reinforced concrete (RC) and fiber reinforced concrete (FRC) deep beams in shear. The study depicted that FRC showed excellent shear resistance, while it caused reduction in the beam deformation capacity. Zamri et al [47] experimentally studied the shear capacity of precast half-joint beams with steel fibers reinforced self-compacting concrete. Also, they developed two semi-empirical equations for prediction of the shear strength of precast SCC and SFSCC beam-half joints based on the analysis of failure modes. The two equations revealed a good correlation with the experimental results.

Researchers [48,49] have studied the nonlinear behavior of deep beams using ANSYS program and concluded that ANSYS program can predict the behavior in good accuracy. Researchers [50-57] have analytically studied the behavior of deep beams using different methods, whereas other researchers [[58–67] have experimentally studied the behavior of deep beams and the effect of different variables on its response.

2. Experimental program

2.1. Description of tested beams

In this study, the experimental program consists of eight RC deep beams with shear span to total depth ratio (a/h) equal to one. The specimens were selected in a way that covers the range of different parameters. All beams dimensions are 150 mm width, 800 mm total depth and 2200 mm length with clear span of 2000 mm. The beams were simply supported and tested in four-points loading arrangement as shown in Figs. 1 and 2. Table 1 summarizes the tested beams data. The deflection was measured by using LVDT. The volumetric ratios of the used hooked end steel fibers in concrete mix were 0.0 %, 0.5%, 0.75%, and 1.0%, respectively. Lengths of steel fibers were 40, 50 and 60 mm with diameter 0.8 mm. The steel fibers aspect ratios (L_f / Φ $_f$) were 50, 62.5 and 75. The mechanical properties of concrete are shown in Table 2 and Fig. 3.

The properties of the reinforcement steel are shown in Table 3 and Fig. 4. Steel reinforcement bars of 16 mm diameter were used in the tension zone and 10 mm diameter steel reinforcement bars were used in compression zone for all beams. The amount and spacing of vertical and

Table 2
Mechanical properties of concrete.

Beam	Experimental cubic compressive strength, f_{cu} (MPa)	Experimental cylindrical compressive strength, f_c'(MPa)	Experimental tensile splitting strength, f_t (MPa)	Strain at maximum compressive strength, ε_0(-)
B1	28.2	23.27	2.54	0.00313
B2	33.0	27.88	2.92	0.00288
B3	33.0	27.88	3.00	0.00288
B4	33.0	27.95	3.00	0.00288
B5	35.0	29.75	3.32	0.00294
B6	36.0	31.11	3.36	0.00273
B7	34.0	28.94	3.21	0.00346
B8	32.0	27.34	3.40	0.00295
Average	33	28	3.10	0.00294
Standard deviation	2.18	2.13	0.27	0.00021

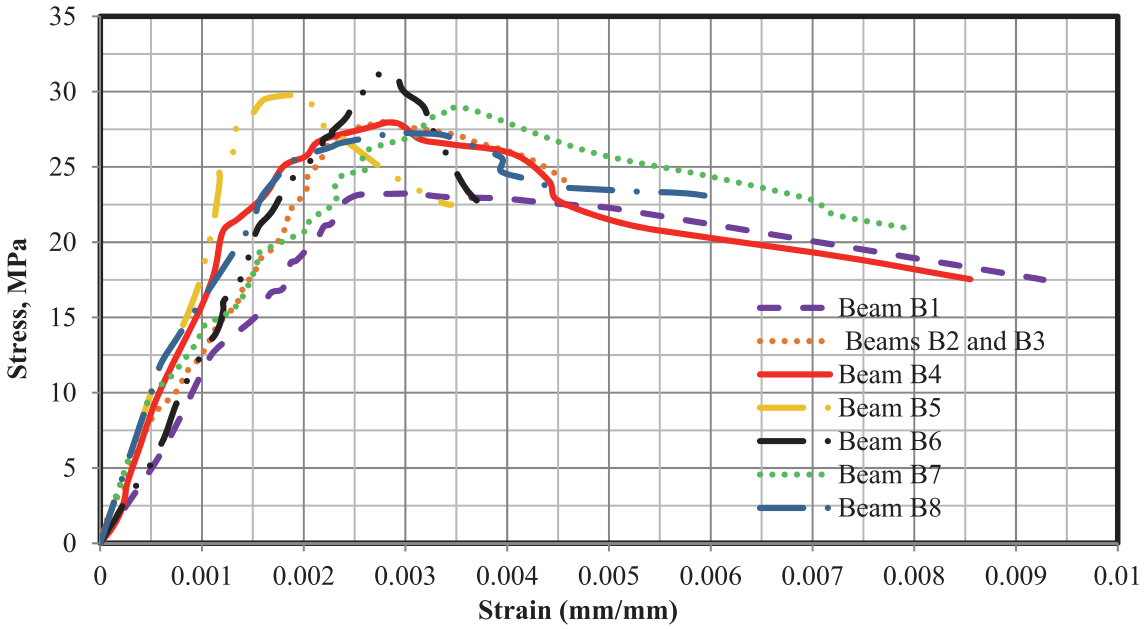

Fig. 3. Concrete compressive stress–strain curves.

Table 3
Mechanical properties of the reinforcement steel bars.

Diameter (mm)	Actual Area* (mm^2)	Yield Strength (Proofing Strength at 2 % Strain) (MPa)	Strain at yield strength, ε_y	Ultimate strength, f_u (MPa)	Elongation %	Young's modulus, E_s (GPa)
8	48.40	334	0.00172	463	15.4	200
10	78.40	553	0.00276	699	13.8	200
16	197.88	550	0.00275	706	12.0	200

*Actual area = Weight of a certain length of reinforcement steel bar/ (Bar length * steel reinforcement specific weight).

horizontal web reinforcement were designed by the Egyptian code (ECP 203). Vertical and horizontal web reinforcement were of 8 mm diameter with spacing 75 mm. Twenty-millimeter concrete cover was maintained and the process was under guidance of professional bar benders.

2.2. Mixture composition and materials properties

The deep beams were constructed using LWFC with a target 28-day cylindrical compressive strength of 28 MPa. The tested beams and material properties were designed according to the ECP 203–2017 [1] and ACI 318–19 [2]. Table 4 shows the mix proportion by weight of the quantities for one cubic meter of concrete to achieve the target compressive strength. Solid foam from Sika company has been used as partial replacement of aggregate to obtain lightweight concrete. The materials used in this program include ordinary Portland cement (OPC), sand, coarse aggregates, solid foam, steel fibers, Sika air, Silica fume, super plasticizer and water. The specific gravity for the used materials is shown in Table 5. Super plasticizer (Sikament, N.N (Sika product)), coarse aggregate and natural siliceous gravel with 10 mm maximum size were used. Steel fibers with hooked end with constant diameter of 0.8 mm has tensile strength 1000 MPa (obtained from the technical data sheet provided by the manufacture) were used. Three cubes (150X150x150 mm) and six cylinders (150 mm diameter and 300 mm height) were cast from each specimen batch and tested at the day of testing of the specimens. The cube was used to determine concrete cubic compressive strength (f_{cu}). Three cylinders were used to determine concrete cylindrical compressive strength (f'_c) according to ASTM C39 [68]. The three cylinders were used to draw stress–strain curves for concrete in compression, determine the strain at the maximum compressive strength and the concrete elastic modules according to

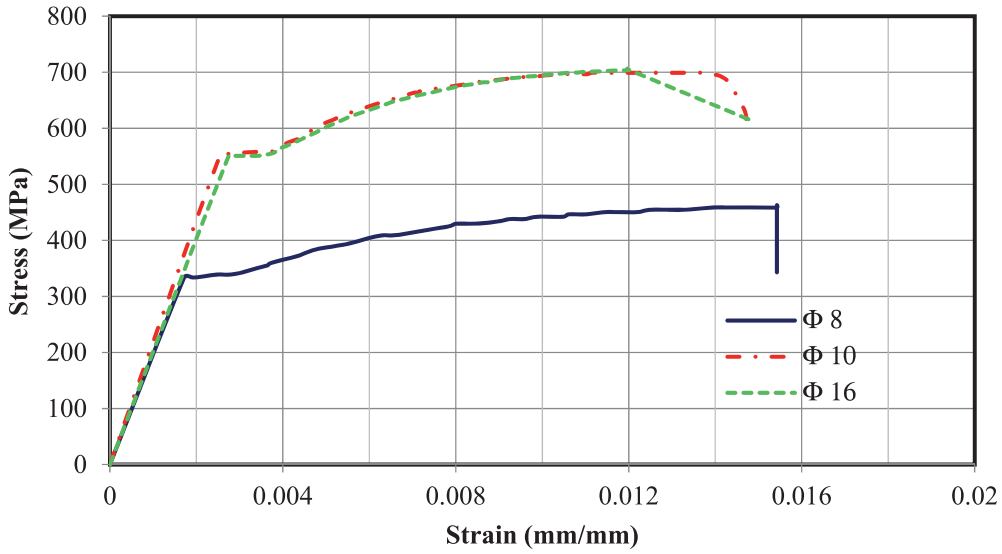

Fig. 4. Steel reinforcement stress–strain curves.

Table 4
Concrete mix design for one cubic meter.

Type	Cement	Sand	Aggregate	Sika Air	Silica Fume	Foam	Super-Plasticizer	Water
Weight (kg)	450	400	510	0.75	50	21	5	185

Table 5
Specific gravity of the used materials.

Cement	Sand	Aggregate	Sika Air	Silica Fume	Foam	Super-Plasticizer	Water
3.15	2.63	2.65	1.01	2.2	0.07	1.15	1

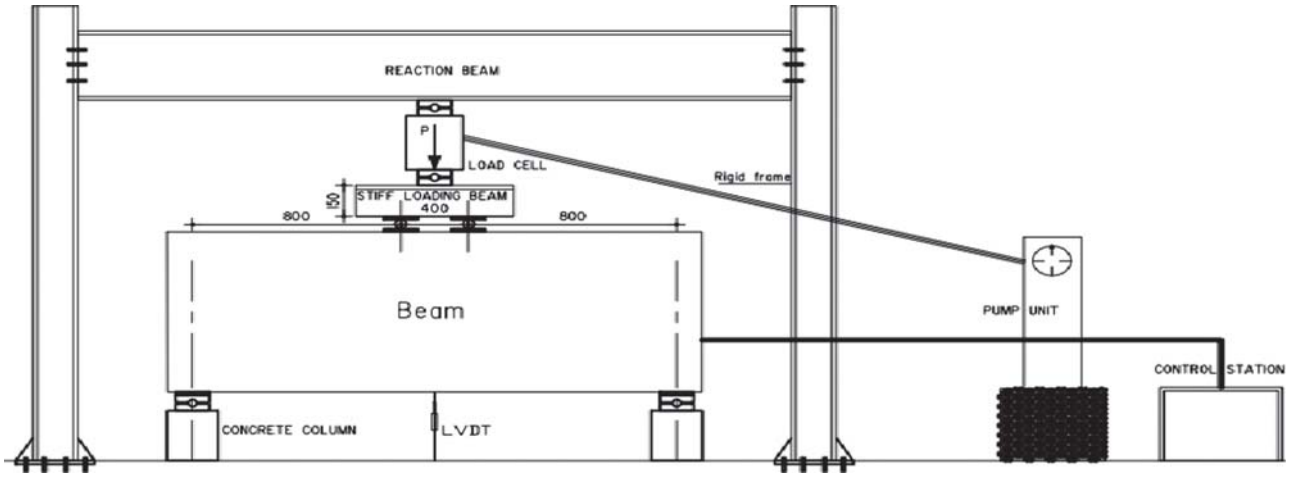

Fig. 5. Test setup and instrumentation.

ASTM C1232 [68]. In addition, three cylinders were used to find the concrete tensile strength from splitting tensile test according to ASTM C496 [68]. The average cubic and cylindrical concrete compressive strength were 33 and 28 MPa, respectively, while the average concrete tensile strength was 3.10 MPa as shown in Table 2. The tensile strength for steel reinforcement bars was determined according to ASTM E8 [68]. The mechanical properties of the reinforcement steel bars are shown in Table 3 and Fig. 4.

2.3. Test setup, instrumentation and test procedure

External measuring apparatuses were attached to the beams in order to obtain the overall deformations and the applied vertical loads. Deflection was measured by Linear Variable Differential Transducers (LVDT) connected to the beam as shown in Fig. 5. The load cell and LVDTs were attached to data logger system in order to record all results through the test stages. Before starting the test, the load cell and LVDT were calibrated, then their initial values were reset to zero through the

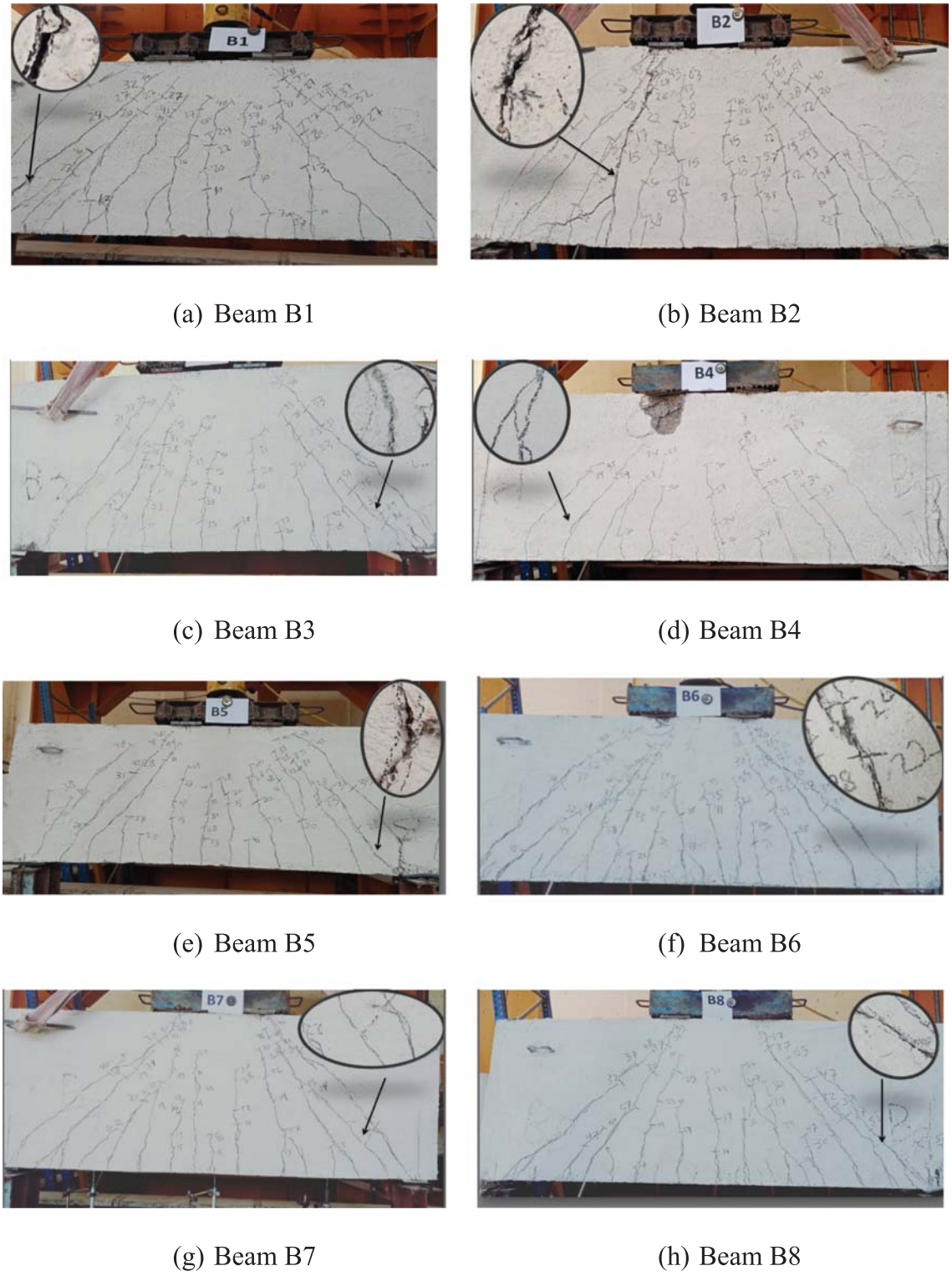

(a) Beam B1 (b) Beam B2

(c) Beam B3 (d) Beam B4

(e) Beam B5 (f) Beam B6

(g) Beam B7 (h) Beam B8

Fig. 6. Cracking patterns for tested beams.

Table 6
Experimental results.

	Experimental Results						
Beam No.	P_{crfm} (kN)	P_{crs} (kN)	$P_{u\ exp.}$ (kN)	$\Delta_{u\ exp.}$ (mm)	Displacement Ductility (mm/mm)	Toughness (kN.mm)	Failure Mode
B1	200	270	565.60	3.22	1.23	729	SBF
B2	220	300	627.70	4.14	1.30	1338	SFW
B3	250	320	791.10	5.16	1.61	1941	SFW
B4	260	340	890.00	5.20	1.70	2563	SFW
B5	250	310	663.80	5.78	1.31	1979	SFW
B6	270	320	710.00	4.35	1.31	1990	SFW
B7	250	310	640.00	3.71	1.32	1351	SFW
B8	210	290	613.31	4.63	1.29	1300	SFW

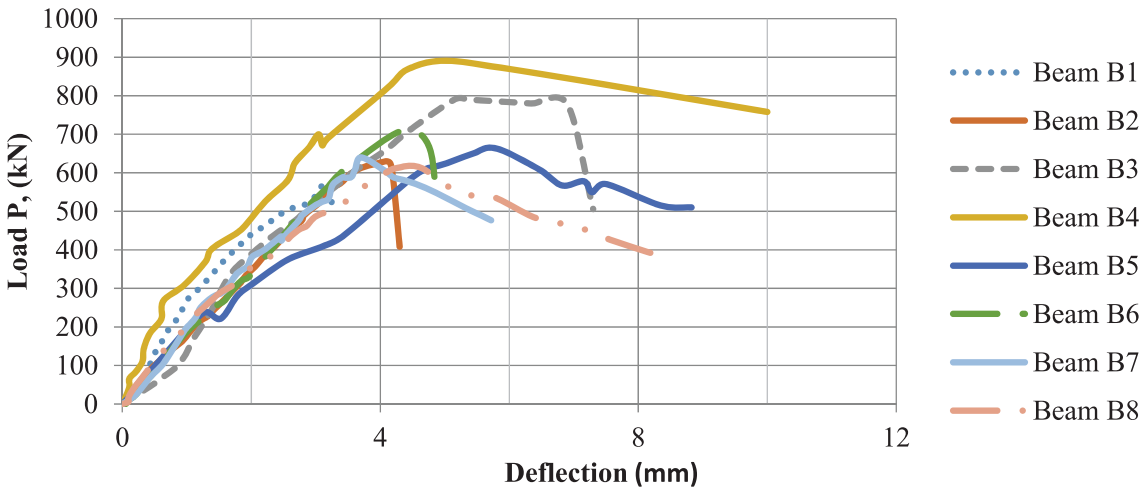

Fig. 7. Load-deflection relationship for all tested beams.

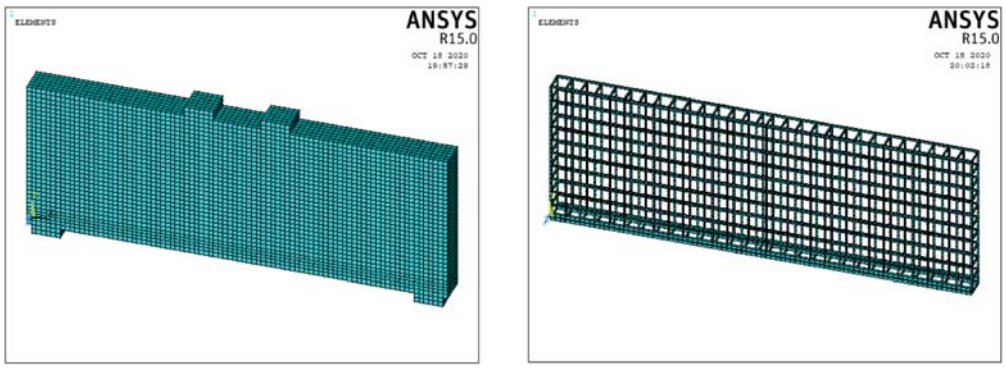

(a) Concrete elements (Solid65) (b) Reinforcing bar elements (Link8)

Fig. 8. ANSYS idealization for deep beams B3 and B4.

lab program. The tested beam was placed under the test set-up as shown in Fig. 5 and the axis of applied load was aligned with the load cell axis to achieve the specific required horizontal distances. All beams were examined under displacement control technique. The beams were tested up to failure under two equals incremental vertical displacement. The vertical displacement rate was chosen to range from 0.20 to 0.50 mm per minute depending on the stiffness of the beam. Data were recorded for the entire duration of the test, while loading was paused for observations and mark cracks.

3. Experimental results

3.1. Cracking pattern

The crack patterns for all tested beams are shown in Fig. 6. The tested beams were initially uncracked in the early stages of loading. Few initial cracks were vertical and perpendicular to the direction of the maximum tensile stress at mid-span. The initial shear cracks, diagonal or inclined were developed near the support in the shear span, and they are induced by the bending moment formed by load increase in range of 29 % to 39 % of the ultimate load. Moreover, it was depicted that the cracks did not penetrate the compression zone.

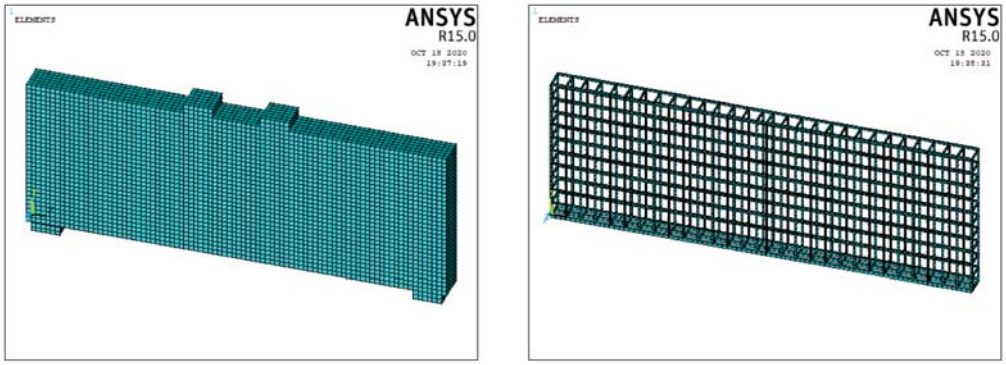

(a) Concrete elements (Solid 65) (b) Reinforcing bar elements (Link 8)

Fig. 9. ANSYS idealization for deep beams B1, B2, B5, B6, B7 and B8.

Table 7
Material properties of the studied beams.

Material	E (GPa)	ν (-)	$f_c^{'}$ (MPa)	f_t (MPa)	f_y (MPa)	E_t (GPa)	Open shear transfer coef. (-)	Closed shear transfer coef. (-)
Fibrous concrete	21	0.20	28	3.1	—	—	0.2	1.0
Steel reinforcement for tested beam	200	0.30	——	—	550	20	—	—
Supports and loading plates	2000	0.25	——	—	——	———	———	———

Where. E. Modulus of elasticity, ν: Poisson's ratio, $f_c^{'}$: Concrete strength, f_t: Tensile splitting strength, f_y: Steel yield strength, E_t: Tangent modulus.

The cracks acquired some inclination towards the central zone, then the main diagonal crack formed in the range of 39 % to 49 % of the ultimate load defining the main diagonal concrete strut. At a loading of 75% of the ultimate load, no cracks appeared but only widening of the existing diagonal cracks (0.50 mm to 2 mm), then the diagonal strut crushed. Failure of beams took place after the full development of the primary diagonal cracks between the load and the support regions, and after the yield of the main steel as shown from the load–deflection plato.

All beams failed in shear with brittle failure mode. Beam B1 (control specimen without fibers) exhibited first crack at 200 kN, while beam B2 (control beam with steel fibers), had first crack at 220 kN. Therefore, the use of steel fibers has increased the first crack load by about 10%. The increase of the reinforcement ratio of the main longitudinal bars for beams B3 and B4 compared to the control beam B2 led to control of diagonal crack width that was monitored and measured using crack width ruler. Comparing the cracks at the same load for beams B3 and B4 to the control beam B2 revealed that the crack width decreased by 31% and 24%, respectively. For beams B2, B5 and B6 with steel fibers volumetric percentage V_f = 0.50 %, 0.75% and 1.0%, the first crack started at 35%, 32% and 29% of its ultimate load. For beams B8, B2 and B7 with steel fibers aspect ratio L_f/Φ_f = 50, 62.5 and 75, the first crack started at 34%, 35% and 38% of the ultimate load as shown in Table 6.

Where:

Displacement ductility: is the ratio of the displacement at 90 % of the ultimate load in the descending branch to that in the ascending branch;
Toughness: is the ability to adsorb deformations up to failure which equals the area under the load–deflection curve up to ultimate;
SBF: is shear brittle failure; and
SFW: shear failure with some warning.

3.2. Failure modes

In this work, all beams failed with shear failure mode, and this is common in deep beams. Fig. 6 shows the crack patterns for all tested beams. Beam B1 failed in a brittle shear failure mode. Beams B2, B3, B4, B5 and B6 failed as a shear failure with some warnings characterized by splitting of concrete along the line joining the loading pad and the beam support. For beams B7 and B8, a splitting occurred when a main crack developed to split the beams from the top (at the loading plate) to the bottom (at supports). Also, beams B7 and B8 exhibited crushing shear failure mode; where the diagonal cracks crushed the concrete strut.

3.3. Load deflection curves and ultimate loads

Fig. 7 shows the load – deflection curves for all tested beams. The load deflection curves showed almost linear uncracked response up to the first crack, and became nonlinear beyond that. An increase in the ultimate load capacity and deflection at the ultimate load was observed in LWFRC beams with steel fibers when compared with non-fibrous concrete beam. This is an indication for the imparted post-cracking ductility.

The increase in the ultimate load was 11.0%, 17% and 26% for beams B2, B5 and B6 with steel fibers content 0.50 %, 0.75 % and 1 %, respectively compared to beam B1 without steel fibers. The increase of steel fibers volume content from 0.5 % (Beam B2) to 0.75 % (Beam B5) and to 1.0 % (Beam B6) increased the displacement ductility by 0.8% and 1.0 %, respectively and increased the toughness by 48 % and 49 %, respectively.

Twenty five percent increase in the steel fibers aspect ratio (L_f/Φ_f) (beam B2 compared to beam B8) increased the first crack load, the ultimate load, displacement ductility and toughness by 5 %, 4%, 2 % and

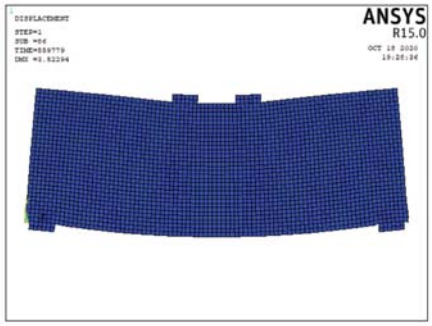

(a) Deformed shape of beam B1

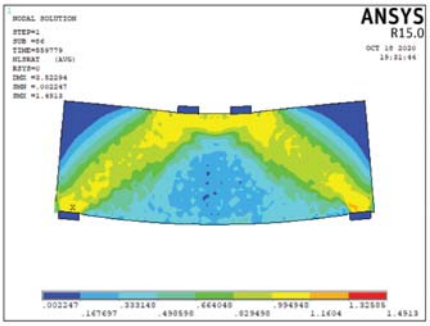

(b) Stress-contours of beam B1

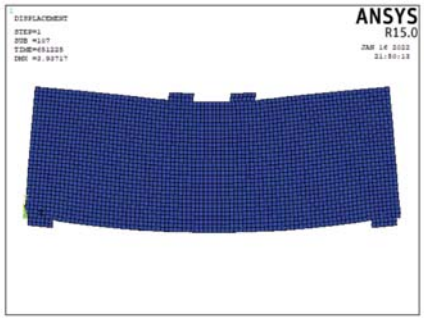

(c) Deformed shape of beam B2

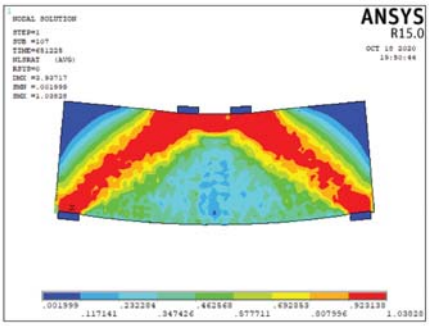

(d) Stress-contours of beam B2

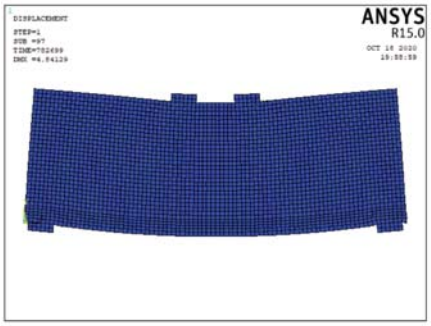

(e) Deformed shape of beam B3

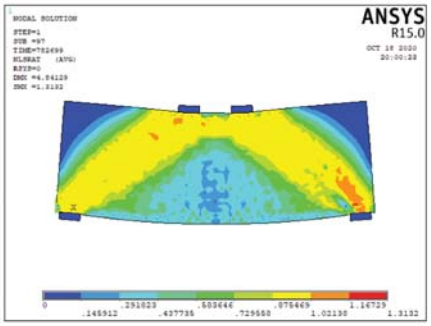

(f) Stress-contours of beam B3

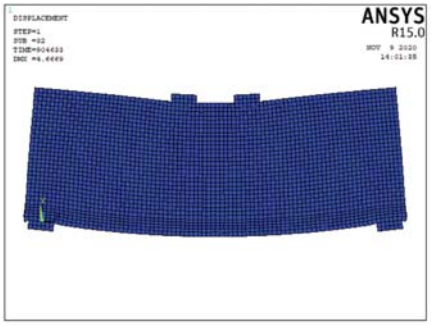

(g) Deformed shape of beam B4

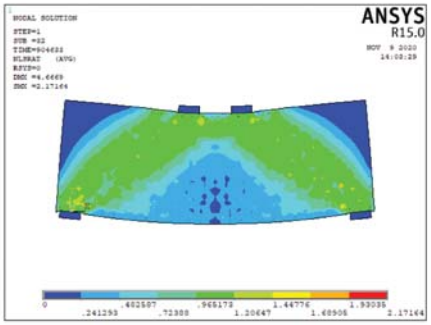

(h) Stress-contours of beam B4

Fig. 10. Deformed shapes and stress contours for all tested beams.

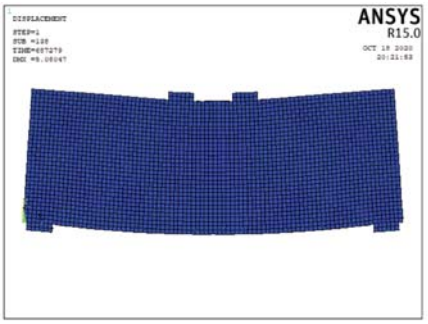

(i) Deformed shape of beam B5

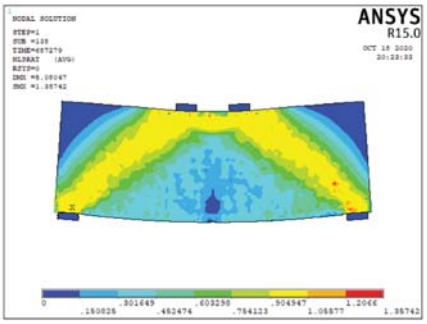

(j) Stress-contours of beam B5

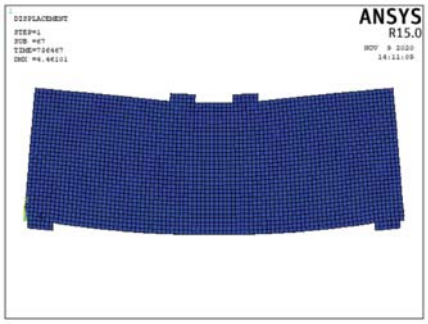

(k) Deformed shape of beam B6

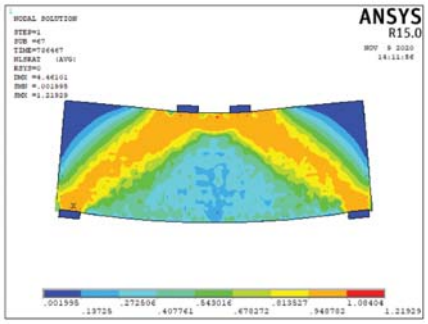

(l) Stress-contours of beam B6

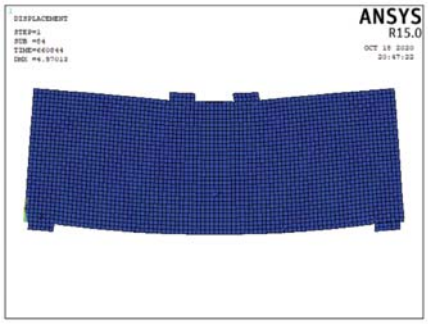

(m)Deformed shape of beam B7

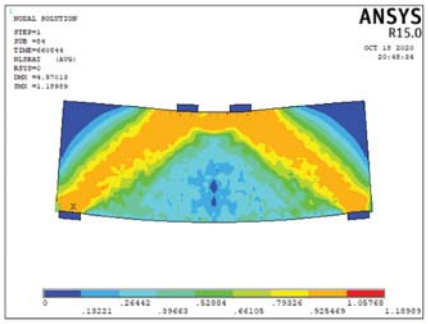

(n) Stress-contours of beam B7

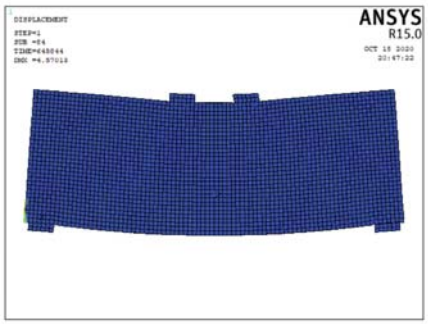

(o) Deformed shape of beam B8

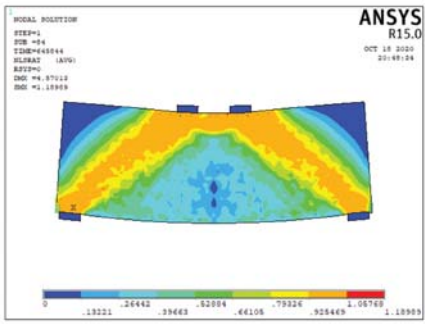

(p) Stress-contours of beam B8

Fig. 10. (*continued*).

Table 8
Predicated results from FE and STM.

Beam No.	FE				STM	
	$P_{crf\ FE}$ (kN)	$P_{crs\ FE}$ (kN)	$P_{u\ FE}$ (kN)	$\Delta_{u\ FE}$ (mm)	$P_{u\ STM}$ [1] (kN)	$P_{u\ STM}$ [2] (kN)
B1	214.20	287.00	559.70	3.60	519.30	573.30
B2	231.70	291.78	651.20	3.93	613.10	614.20
B3	241.70	311.78	782.70	4.84	847.30	800.50
B4	254.28	358.97	904.00	4.66	1016.80	1030.00
B5	251.70	297.41	687.20	5.08	639.30	634.60
B6	259.28	314.28	736.47	4.46	654.30	643.30
B7	240.50	275.22	660.00	3.79	620.80	622.60
B8	216.00	263.66	638.84	4.56	600.30	614.30

2.8 %, respectively, whereas 50 % -increase in $L_f/\ \Phi_f$ (beam B7 compared to B8) resulted in and increase19 %, 4 %, 2 % and 3.9 %, respectively. This means that the fiber aspect ratio showed no effect on the ultimate load, displacement ductility and toughness.

The increase of the main longitudinal steel reinforcement ratio by 33% and 66% (Beams B3 and B4) increased the ultimate shear capacity by 25 % and 41%, respectively compared to that of the control beam B2 with steel fibers, increased the displacement ductility by 24% and 30 %, respectively, and increased the toughness by 45.0 % and 92 %, respectively.

4. Numerical analysis

In this study, nonlinear analysis program ANSYS V. 15 is used to create the numerical simulation. An eight-node solid element (SOLID65) was used for concrete modeling as shown in Figs. 8 and 9, with three translational and additional rotational degrees of freedom at each node. Special features of SOLID65 are taken into consideration such as; plasticity, cracking, creep, large strain, large deflection, and capability of plastic deformation. The used mesh size for modeling the beams is 25x25x25mm. Link8 element was used to model the steel reinforcement which has two nodes with three degrees of freedom-translations at each node at X, Y and Z directions. The bond between steel reinforcement and concrete is assumed to be perfected bond. The effect of fibers is taken through properties of the fibrous concrete (E, ν, f'_c, f_t), open and closed shear coefficient as shown in Table 7.

Fig. 10 shows the deformed shape and the contours of the stresses for all tested beams.

The strut and tie method (STM) is used for the design of disturbed region (D-regions). In this paper, the STM method for LWFRC deep beam with steel fibers was applied in accordance with the ECP 203–2017 [1] and ACI 318–19 [2]. The effect of steel fibers volume (V_f), steel fibers aspect ratio ($l_f/\ \Phi_f$) and main steel reinforcement ratio is considered. The angle between the axis of the strut and the tie (θ) should be as large as possible to avoid incompatibilities and reduce cracking due to shortening of strut and lengthening of the tie occurred in the same direction.

5. Results Comparison

The numerical and analytical results from finite element analysis (FE) and strut and tie model (STM) are shown in Table 8. The numerical results from FE and the experimental results are plotted in Fig. 11. Comparison of the experimental, numerical and analytical results showed a good agreement; where the mean, standard deviation of the predicted and measured values of P_{crf}, P_{crs}, P_u and Δ_u shown in Table 9 are in the acceptable range. The mean of ($P_{crf\ FE}/P_{crf\ exp.}$), ($P_{crs\ FE}/P_{crs\ exp.}$), ($P_{u\ FE}/P_{u\ exp.}$), ($\Delta_{u\ FE}/\Delta_{u\ exp.}$), ($P_{u\ STM}$ [1]$/P_{u\ exp.}$) and ($P_{u\ STM}$ [2]$/P_{u\ exp.}$) are 100.44 %, 97.55 %, 102.27 %, 95.70 %, 99.27 % and 99.97 %, respectively. The load–deflection curves for beams B7 and B8 from the numerical results were very similar to that of the experimental ones. The standard deviation of the loads level stayed below 10 %. Table 9 depicted that both the ECP 203–2017 [1] and ACI 318–19 [2] are conservative in calculating the ultimate shear load using STM for specimens (B2, B5, B6 and B8), while being unconservative for specimens (B1, B3, B4 and B7). The ECP 203–2017 [1] is slightly conservative in calculating the ultimate capacity than ACI 318–19 [2] for the range of the studied variables in this research.

Output samples for beams B1 and B2 from both experimental and numerical (FE) results indicating the cracks' propagation are given in Fig. 12. From this figure, it can be noticed that, the measured and predicated cracking patterns are similar. This matching was obtained for all other tested beams.

6. Conclusions

1- The use of 1% steel fibers content in the LWFRC deep beams increased the first crack load by 35%, the ultimate load carrying capacity by 25.5%, the toughness by 124.0% and the displacement ductility by 6.5% when comparing with a beam without steel fibers.
2- The increase of steel fibers volumetric percentage by 50% increased the first crack load, the ultimate load, the displacement ductility and the toughness by 14%, 6%, 0.77% and 48%, respectively. The increase of steel fibers volumetric percentage by 100% increased the first crack load, the ultimate load, the displacement ductility and the toughness by 23%, 13%, 1.5% and 49%, respectively.
3- Steel fibers aspect ratio showed an insignificant effect on the cracking load, ultimate load, displacement ductility and toughness of LWFRC deep beams.
4- Main reinforcement steel ratio and steel fibers volumetric percentage has significant effect on the cracking load, ultimate load, displacement ductility and toughness of the LWFTC deep beams. Increasing the main reinforcement ratio by 33% and 66% increased the cracking load by 14 % and 18 %, the ultimate load by 26% and 42%, the displacement ductility by 24% and 31% and the toughness by 45% and 92%.
5- The experimental results and the nonlinear finite element results using ANSYS program showed a good agreement, where the mean value of the predicted cracking load, ultimate load and displacement at ultimate load is 97.55%, 102.22% and 97.65%, respectively with standard deviation less than 6% compared to the measured values.
6- Both, Egyptian and American codes are slightly conservative in calculating the ultimate capacity for the range of the studied variables in this research.
7- The failure modes of all tested fibrous reinforced concrete beams were shear failure with some warnings accompanied with clear flexural cracks. For non-fibrous reinforced concrete beam, the failure was shear brittle failure mode.

Declaration of Competing Interest

The authors declare that they have no known competing financial interests or personal relationships that could have appeared to influence the work reported in this paper.

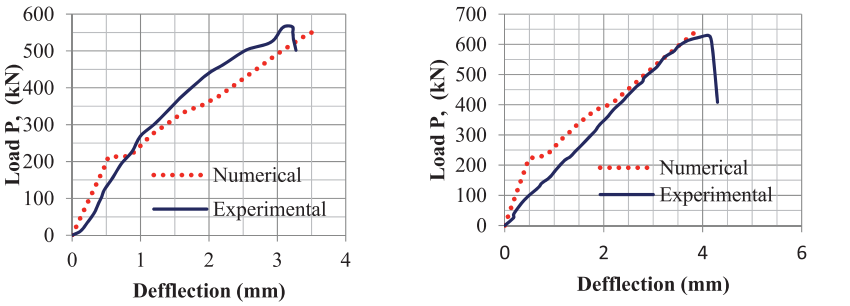

(a) Beam B1 (b) Beam B2

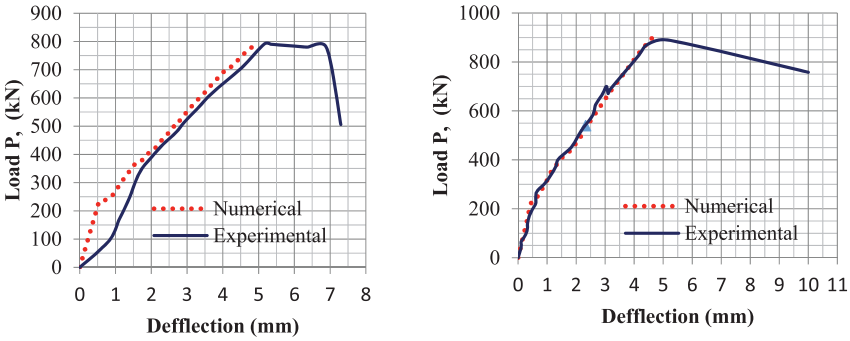

(c) Beam B3 (d) Beam B4

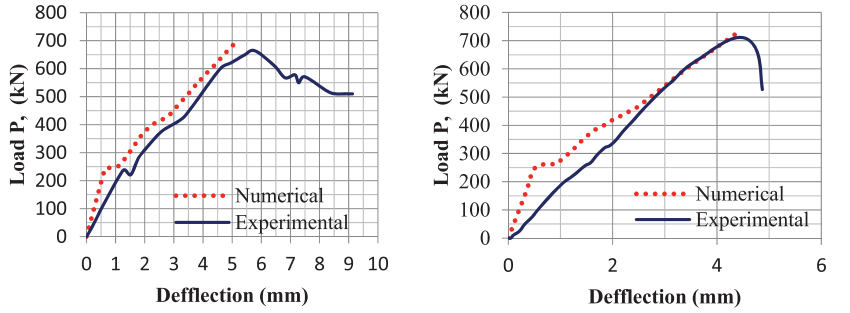

(e) Beam B5 (f) Beam B6

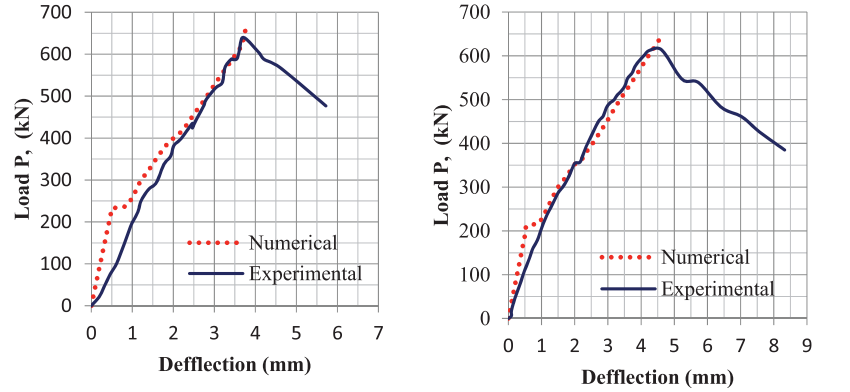

(g) Beam B7 (h) Beam B8

Fig. 11. Experimental and numerical load–deflection curves.

Table 9
Comparison between experimental, numerical and analytical results.

Beam No.	B1	B2	B3	B4	B5	B6	B7	B8	Mean	Standard Deviation
$P_{crf\ FE}$ / $P_{crf\ exp.\%}$	107.10	105.32	96.68	97.80	100.68	96.03	96.20	102.86	100.33	4.07
$P_{crs\ FE}$ / $P_{crs\ exp.\%}$	106.30	97.26	97.43	105.58	95.94	98.21	88.78	90.92	97.55	5.76
$P_{u\ FE}$ / $P_{u\ exp.\%}$	98.96	103.74	98.94	101.57	103.53	103.73	103.13	104.16	102.22	2.02
$\Delta_{u\ FE}$ / $\Delta_{u\ exp.\%}$	111.80	94.93	93.80	89.62	87.89	102.53	102.16	98.49	97.65	7.16
$P_{u\ STM}$ [1]/$P_{u\ exp.\%}$	91.81	97.67	107.10	114.25	96.31	92.15	97.00	97.88	99.27	7.16
$P_{u\ STM}$ [2]/$P_{u\ exp.\%}$	101.36	97.85	101.18	115.73	95.60	90.61	97.28	100.16	99.97	6.80
P_{uSTM} [1]/P_{uSTM} [2]%	90.58	99.82	105.85	98.72	100.74	101.71	99.71	97.70	99.35	4.03

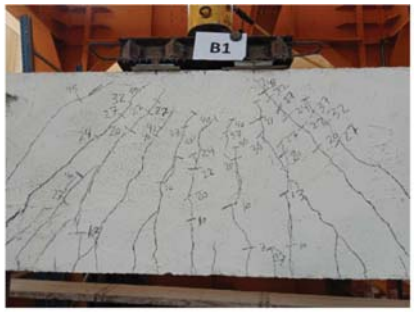

(a) Experimental crack pattern for Beam B1

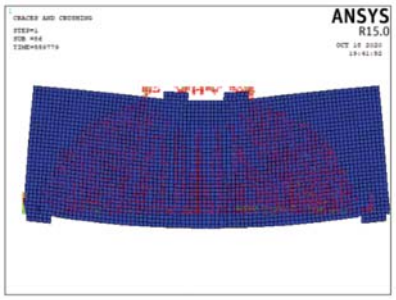

(b) Numerical crack pattern for Beam B1

(c) Experimental crack pattern for Beam B2

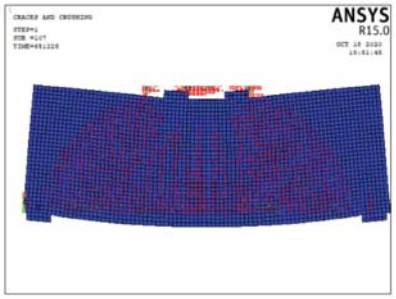

(d) Numerical crack pattern for Beam B2

Fig. 12. Experimental and numerical cracks propagation for beams B1 and B2.

References

[1] Egyptian Code of Practice for Design and Construction of Reinforced Concrete Structures ECP-203, Housing and Building Research Center, Ministry of Building and Construction, Giza, Egypt, 2017, Chapter 6, pp. 113-122.

[2] ACI Committee 318-19, Building Code Required for Reinforced Concrete, (ACI 318-19) and Commentary (ACI 318R-19), American Concrete Institute, Farmington Hills, Mich,2018.

[3] AL-Kasasbeh, T., and Allouzi, R., "Behavior of polypropylene fiber foamed reinforced concrete beams laterally reinforced with/without glass fiber grid", International Journal of Structural Integrity, 9864-1757, 2020.

[4] Mohamed A, El Madawy ME, Chung SY, Sikora P, Stephan D. Preparation and characterization of ultra-lightweight foamed concrete incorporating lightweight aggregates. Journal of Applied Sciences 2019;9(7):1447.

[5] Lim SK, Tan CS, Li B, Ling T, Hossain MU, Poon CS. Utilizing high volumes of quarry wastes in the production of lightweight foamed concrete. Journal of Construction Building Materials 2017;151:441–8.

[6] Hilal AA, Thom NH, Dawson AR. On void structure and strength of foamed concrete made without/with additives. Journal of Construction Building Materials 2015;85:157–64.

[7] Lee, Y., "Flexural behavior of reinforced lightweight foamed mortar beams and slabs", KSCE, Journal of Civil Engineering, pp. 1817-1822, 2017.

[8] Tan, J.H., Lim, S.K., and Lim, J.H., "Flexural behavior of reinforced lightweight foamed concrete beams", Kuala Lumpur, Malaysia, ISSN: 2395-0072 Vol. 5, 2017.

[9] Scholar MT. Experimental study on foamed concrete. International Journal of Civil Structural Environmental and Infrastructure Engineering Research and Development, IJCSEIERD 2014;4(1):145–58.

[10] Hilal, A.A., Thom, N.H., and Dawson, A.R., "Foamed concrete: from weakness to strength", International 34th Cement and Concrete Science Conference, University of Sheffield: England, pp. 105-108, 2014.

[11] Devansh, J., Hindoriya, A.K., and Bhadauria, S.S., "Evaluation of properties of cellular lightweight concrete", AIP Conference Proceedings, AIP Publishing LLC, 2019.

[12] Chundakus, H., Diharjo, K., Setyono, P., and Satwiko, P., "Study of characteristic physical and mechanic of foamed lightweight concrete with fly ash added for wall materials", International Journal of Recent Engineering Science (IJRES), Vol. 5, No. 1, 2018.

[13] Huei, L.Y., and Satwiko, P., "Compressive strength of lightweight foamed concrete with charcoal as a sand replacement", Indian Journal of Engineering and Materials Sciences, Vol. 25, No. 1, 2018. .

[14] Risdanareni, P., Sulton, M., and Nastiti, S.F, "Lightweight foamed concrete for prefabricated house", AIP Conference Proceedings, 2016. .

[15] Camille L. Investigating the fire resistance of ultra-lightweight foamed concrete. Technical Journal of the Faculty of Engineering University of Zulia 2014;37(1): 11–8.

[16] Sarje HK, Autade AS. Consequences of protein based foaming agent on lightweight concrete. International Journal of Recent Technology and Engineering (IJRTE), ISSN 2014;3(5):2277–3878.

[17] Solikin, M., and Ikhsan, N., "Styrofoam as partial substitution of fine aggregate in lightweight concrete bricks", AIP Conference Proceedings, AIP Publishing LLC, 2018.

[18] Shaaban IG, Zaher AH, Said M, Montaser W, Ramadan M, Abd El-Hameed GN. Effect of partial replacement of coarse aggregate by polystyrene balls on the shear behavior of deep beams with web openings. Case Stud Constr Mater 2020;12: e00328.

[19] Aisswarya R. Experimental Analysis of Light Weight Concrete. IJASRE 2018;4(7): 65–73.

[20] Abhijeet, P., and Mehetre, A.J., "Evaluation of effectiveness of SFRC deep beams in shear", International Journal of Research Studies in Science, Engineering and Technology, Vol. 2, No. 7, 2015.

[21] Ganesan N, Indira PV. Engineering properties of steel fibers reinforced geopolymer concrete. Journal of Advances in Concrete Construction 2013;1(4):305.

[22] Balgude MR, Vijaysinh V. Experimental study on crimped steel fibers reinforced concrete deep beams in shear. IOSR Journal of Mechanical and Civil Engineering 2014;11(2):24–39.

[23] Nipurte O, Patil L, Patil P, Potinda V. Study of behavior of steel fibers reinforced concrete in deep beams for flexure. IJSRSET, International Journal of Scientific Research in Science, Engineering and Technology, ISSN 2018;4(1):2395–4099.

[24] Pujadas, P., Blanco, A., Cavalaro, S., De la Fuente, A. and Aguado, A., "Flexural post-cracking creep behavior of macro-synthetic and steel fibers reinforced concrete", International RILEM Workshop on Creep Behavior in Cracked Section of Fiber Reinforced Concrete, pp. 77-87, 2017.

[25] Song PS, Hwang S. Mechanical properties of high-strength steel fibers-reinforced concrete. Constr Build Mater 2004;18(9):669–73.

[26] Yazici Ş, İnan G, Tabak V. Effect of aspect ratio and volume fraction of steel fibers on the mechanical properties of SFRC. Constr Build Mater June 2007;21(6): 1250–3.

[27] Hao Y, Hong H. Pull-out behavior of spiral-shaped steel fibers from normal-strength concrete matrix. Constr Build Mater 2017;139:34–44.

[28] Shengli, Z, Changsuo, Z and Lin, L.," Investigation on the relationship between the steel fibers distribution and the post-cracking behavior of SFRC", Construction and Building Materials, 2019, Vol. 200, pp. 539-550.

[29] Raju RA, Lim S, Akiyama M, Kageyama T. Effects of concrete flow on the distribution and orientation of fibers and flexural behavior of steel fibers-reinforced self-compacting concrete beams. Constr Build Mater 2020;262:119963.

[30] Gou H, Zhu H, Zhou H, Yang Z. Reinforcement mechanism of orientally distributed steel fibers on ultra-high-performance concrete. Constr Build Mater 2021;281: 122646. https://doi.org/10.1016/j.conbuildmat.2021.122646.

[31] Humnabad, A. N., and Autade, P.B., "Experimental evaluation shear strength of steel fibers reinforced concrete deep beams", International Journal of Engineering Research and Technology (IJERT), 5.05, 2016. .

[32] Demir, A., Ozturk, H., Edip, K., Stojmanovska, M. and Bogdanovic, A., "Effect of viscosity parameter on the numerical simulation of reinforced concrete deep beams behavior", The Online Journal of Science and Technology, Vol. 8, No. 3, 2018.

[33] Mohamed, K., Farghaly, A.S. and Benmokrane, B., "Proposed strut-and-tie model for concrete deep beams reinforced with FRP bars", Canada Research Chair in Advanced Composite Materials for Civil Structures, June 1–4, 2016.

[34] Vilar MMS, Sartorato M, Santana HB, Leite MR. Finite elements numerical solution of deep beams based on layer wise displacement field. J Braz Soc Mech Sci Eng 2018;40(9):477.

[35] Kulkarni, S.K., Kekade, G. and Halkude, S.A., "Experimental study on hybrid fiber reinforced concrete deep beams", International Journal of Civil Engineering (SSRG-IJCE)- Vol. 4, No. 2, 2017.

[36] Magdalene, P.S. and Kanmani, V., "Experimental and numerical study of deep beams by finite element method (FEM)", Journal of Engineering Research and Application, ISSN: 2248-9622, Vol. 8, No.7 ,(Part-II), 2018.

[37] Santos DP, Neto F, Reginato JAD, Carrazedo RI. Optimized design of RC deep beams based on performance metrics applied to strut and tie model and in-plane stress conditions. Latin American Journal of Solids and Structures 2019;16:7.

[38] Agus S, Taufik S. Numerical modelling behavior of reinforced concrete deep beams with strut-and-tie model. International Journal of Mechanical Applications 2008;8: 1–9.

[39] Aaron, C.B., Wilson, K. E., Bayrak, O., and Russo, F.M., "Strut-and-tie modeling (STM) for concrete structures, design examples", FHWA-NHI-17-071, National Highway Institute (US), 2017.

[40] Mohammad, P., Chai, H.K., and Voo, Y.L., "Refinement of strut-and-tie model for reinforced concrete deep beams", PloS one, June 25, 2015, https://doi.org/ 10.1371/Journal.pone.0130734. .

[41] Adnan AA, Khadhim AM. Studying the behavior of lightweight deep beams with openings. International Journal of Engineering Technologies and Management Research 2019;6(12):89–100.

[42] Karolína T. Two parameters kinematic approach for the shear behavior of deep beams made of fiber-reinforced concrete. Master Theses, Faculty of Sciences Applications, European Mundus - 2017;11134:528.

[43] Deng M, Ma F, Ye W, Liang X. Investigation of the shear strength of HDC deep beams based on a modified direct strut-and-tie model. Constr Build Mater 2018; 172:340–8.

[44] Mohammadhassani M, Jumaat MZ, Jameel M. Experimental investigation to compare the modulus of rupture in high strength self-compacting concrete deep beams and high strength concrete normal beams. Constr Build Mater 2012;30: 265–73.

[45] Jang, S. J., Jeong, G. Y., and Yun, H. D.," Use of steel fibers as transverse reinforcement in diagonally reinforced coupling beams with normal-and high-strength concrete", Construction and Building Materials, 2018, Vol. 187, pp. 1020-1030.

[46] Albidah A, Abadel A, Abbas H, Almusallam T, Al-Salloum Y. Experimental and analytical study of strengthening schemes for shear deficient RC deep beams. Constr Build Mater 2019;216:673–86.

[47] Zamri NF, Mohamed RN, Elliott KS. Shear capacity of precast half-joint beams with steel fibers reinforced self-compacting concrete. Constr Build Mater February 2021; 272:121813.

[48] Taufik, S., Anggarini, E. and Setiawan, I.,"ANSYS numerical modeling of confined deep beams with high strength concrete", International Journal of Structural Glass and Advanced Materials Research, Vol. 4: pp. 41.55, 2020.

[49] Douread RH, Samad AAA, Mohamad N, Attiyah AN, Mezher TM, Azeez A. A, "Nonlinear analysis of RC deep beams strengthened with NSM CFRP anchor bars". International Journal of Advanced and Applied Sciences 2018;5(11):61–6.

[50] Mohammadhassani M, Zarrini M, Noroozinejad Farsangi E, Khadem Gerayli N. "Prediction of structural response for HSSCC deep beams implementing a machine learning approach", International Journal of Coastal and Offshore. Engineering 2018;2(1):35–43.

[51] Sri, H.G., and Raju, P.P., "Shear strength of deep beams: a state of Art", International Conference on Advances in Civil Engineering (ICACE-2019), Vol. 21, 2019.

[52] Thomas P, Tharu B. Analytical study on lightweight concrete deep beams. Journal of Transactions on Engineering and Sciences, ISSN 2014;2(10):2347–11964.

[53] Folino P, Ripani M, Xargay H, Rocca N. Comprehensive analysis of fiber reinforced concrete beams with conventional reinforcement. Eng Struct 2020;202:109862. https://doi.org/10.1016/j.engstruct.2019.109862.

[54] Kueres, D., Polak, M. A., and Hegger, J., (2020)," Two-parameter kinematic theory for punching shear in steel fibers reinforced concrete slabs", Engineering Structures, 205, 110086.

[55] Abdul-Razzaq KS, Mustafa Jalil A, Asaad Dawood A. Reinforcing struts and ties in concrete continuous deep beams". Eng Struct 2021;240:112339. https://doi.org/ 10.1016/j.engstruct.2021.112339.

[56] Lin Y, Yan J, Wang Z, Fan F, Yang Y, Yu Z. Failure mechanism and failure patterns of SCS composite beams with steel-fiber-reinforced UHPC. Eng Struct 2020;211: 110471. https://doi.org/10.1016/j.engstruct.2020.110471.

[57] Zhang Y, Liu A, Chen B, Zhang J, Pi YL, Bradford MA. Experimental and numerical study of shear connection in composite beams of steel and steel-fiber reinforced concrete. Eng Struct 2020;215:110707.

[58] Lu W-Y, Hsiao H-T, Chen C-L, Huang S-M, Lin M-C. Tests of reinforced concrete deep beams. Computers and Concrete 2015;15(3):357–72.

[59] Rahimeh, H., and Nolsjo, A., "The effect of reinforcement configuration on crack widths in concrete deep beams", ISSN 1103-4297; 506 DIVA Journal, 2017.

[60] Hassan HM, Arab MAES, el-kassas AI. Behavior of high strength self-compacted concrete deep beams with web openings. Heliyon 2019;5(4):e01524. https://doi.org/10.1016/j.heliyon.2019.e01524.

[61] Kamonna HHH, Shakir QM, Al-Tameemi HA. Behavior of high-strength self-consolidated reinforced concrete t-deep beams. The Open Construction and Building Technology Journal 2020;14(1):51–69.

[62] Hong ZJ, Li SS, Xie W, Guo YD. Experimental study on shear capacity of high strength reinforcement concrete deep beams with small shear span–depth ratio. Journal of Materials 2020;13(5):1218.

[63] Syroka-Korol E, Tejchman J. Experimental investigations of size effect in reinforced concrete beams failing by shear. Eng Struct 2014;58:63–78.

[64] Yaseen, Z. M., Tran, M. T., Kim, S., Bakhshpoori, T., and Deo, R. C., (2018)," Shear strength prediction of steel fibers reinforced concrete beam using hybrid intelligence models: a new approach", Engineering Structures, 177, 244-255.

[65] Zhang, F., Ding, Y., Xu, J., Zhang, Y., Zhu, W., and Shi, Y., (2016)," Shear strength prediction for steel fibers reinforced concrete beams without stirrups", Engineering Structures, 127, 101-116.

[66] Yoo D-Y, Yuan T, Yang J-M, Yoon Y-S. Feasibility of replacing minimum shear reinforcement with steel fibers for sustainable high-strength concrete beams. Eng Struct 2017;147:207–22.

[67] Nguyen HTN, Tan KH, Kanda T. Effect of polypropylene and steel fibers on web-shear resistance of deep concrete hollow-core slabs. Eng Struct 2020;210:110273. https://doi.org/10.1016/j.engstruct.2020.110273.

[68] American Society for Testing and Materials (ASTM), 2001.